Nanoscale

PAPER

View Article Online
View Journal | View Issue

Cite this: *Nanoscale*, 2025, **17**, 3436

Unveiling the potential of Cu–Pd/CdS catalysts to supply and rectify electron transfer for H_2 generation from water splitting†

Ejaz Hussain, *[a] Mamoona Idrees,[a] Muhammad Jalil,[a] Muhammad Zeeshan Abid, [a] Khalid Aljohani[b] and Khezina Rafiq *[a]

As a future fuel, obtaining hydrogen from water could be a game changer for the renewable energy sector, because it has the potential to be used as an alternative to fossil fuels. The current project has been designed to develop catalysts that can produce hydrogen from water on irradiation by sunlight. For this purpose, CdS, Cu/CdS, Pd/CdS, and Cu–Pd/CdS catalysts were successfully synthesised and utilized for hydrogen generation. The catalytic activity of pristine CdS has potentially been enhanced with Cu and Pd cocatalysts that were deposited *via* a chemical reduction strategy. The morphology and optical characteristics were assessed *via* XRD, Raman, UV-Vis/DRS, PL, SEM, HRTEM and AFM techniques. The phase purity, composition and charge transfer were confirmed by EDX, XPS and EIS studies. Under similar conditions, photoreactions and H_2 evolution experiments were performed in a quartz reactor (UK/Velp-Sci) and GC-TCD (Shimadzu, 2014), respectively. Overall, a Cu–Pd/CdS catalyst (0.2% Cu and 0.8% Pd) was found to be the most active, potentially delivering 33.71 mmol g^{-1} h^{-1} of hydrogen. Higher efficiencies were attributed to the existence of Cu and Pd on CdS surfaces. It has been predicted that Cu cocatalysts increase the electron densities on CdS surfaces (*i.e.* active sites), while Pd cocatalysts reduce the back reactions (higher charge transportation) by forming Schottky junctions. Various factors like pH, temperature, intensity of light and catalyst dose are evaluated and discussed. Based on the results and activities, it has been concluded that the described approach shows potential to replace fossil fuels.

Received 17th August 2024,
Accepted 16th November 2024

DOI: 10.1039/d4nr03381g

rsc.li/nanoscale

Introduction

Escalation in population, urbanization and industrialization have all contributed to a significant increase in energy demand. Over the entire world, the cost and consumption of fossil fuels have risen to the extent that they have become unaffordable by undeveloped countries. On the other hand, sources of fossil fuels are finite and non-renewable. Moreover, these resources are specifically limited for developing countries where 70 to 75% of energy demand is covered by these fuels.[1] Another problem is that burning of these fuels produces greenhouse gases. The disadvantage of greenhouse gases is that they are constantly causing global warming. It is understood that a consistent increment in global warming could erase life on Earth.[2] Due to the aforementioned issues and perspectives, alternative fuels have become an urgent necessity for the world. The most promising non-traditional energy source is hydrogen, which does not exist naturally in the free state.[3] Hydrogen is eco-friendly and can be readily used in fuel cells to scale up green energy. Another significant advantage is that it can deliver 2.75 times more energy (*i.e.* 122 kJ g^{-1}) than other traditional fuels.[4] Thus, obtaining hydrogen as a renewable source would be an effective solution to reducing the energy crises.[5] Hydrogen is the most promising fuel to get rid of the excessive use of fossil fuels that are polluting our atmosphere day by day.[6] On planet earth, hydrogen widely exists in the form of water, hydrides, hydrocarbons and biomass. It is the fuel being burnt in the sun as well as in other stars in the universe.

Historically, the first successful attempt at photocatalytic water splitting was achieved by Fujishima and Honda in 1972.[7] After this successful attempt, significant research has been conducted for sunlight-driven catalytic water splitting. Recently, hydrogen has been accepted as an alternative fuel (Energy Policy Act of 1992/USA).[8] Due to its potential for higher energy content, its demand for commercial use has increased surprisingly.[9] However, a main drawback associated with hydrogen is that,

[a]*Institute of Chemistry, Inorganic Materials Laboratory 52S, The Islamia University of Bahawalpur-63100, Pakistan. E-mail: ejaz.hussain@iub.edu.pk, khezina.rafiq@iub.eu.pk*
[b]*Department of Mechanical Engineering, College of Engineering in Al-Kharj, Prince Sattam Bin Abdulaziz University, Al-Kharj, 11942, Saudi Arabia*
† Electronic supplementary information (ESI) available. See DOI: https://doi.org/10.1039/d4nr03381g

relative to fossil fuels, it does not exist in the free state.[10–12] Generally, hydrogen has been produced *via* steam reforming, biomass, and the electrolysis of water. It is worth mentioning that its supply to gas stations needs extra care.[13]

Although several methods like photolysis, thermolysis, combustion, biomass, photo-fermentation and the electrolysis of water have been reported for hydrogen production, they all suffer a number of drawbacks:[14] for example, (i) excessive requirement for electricity, (ii) extra burden of expertise and labour, (iii) cost and accessibility, (iv) impurities and low yield.[15] However, obtaining hydrogen by photocatalytic water splitting is the most promising due to the following advantages: (i) quick and simultaneous delivery, (ii) no need for electricity, (iii) high purity yield, (iv) low cost and renewability.[16,17] Another advantage is that the water splitting reaction can be driven on sunlight without the supply of electricity. But for successful water splitting, the catalysts must have suitable band potentials with regard to the reduction/oxidation potentials of water. To date, several catalysts, for example, TiO_2, ZnO, $SrTiO_3$, $Zn_3V_2O_8$, $CuFe_2O_4$, $BiVO_4$, metal and non-metal doped, g-C_3N_4, graphene, COFs, MOFs and MOF-derived catalysts and MXene-supported catalysts, have been successfully used.[14,18–27] The problem is that all these catalysts have failed due to a number of limitations, including stability, low response in the visible spectrum, structural defects and unsuitable band gaps. The aforementioned catalysts are specifically rejected due to over-potential and charge recombination for an aqueous system. For example, the hydrogen generation activity of bare TiO_2 is limited due to its larger band gap (3.20 eV).[28,29] Relative to TiO_2, CdS is more efficient and can produce hydrogen in the visible spectrum (2.40 eV).[30] It has been confirmed that CdS has enormous catalytic properties, such as a suitable band gap, excellent absorbance and higher photoconductivity.[31] Thus, CdS progressively converts the photon energy of sunlight into active charges (e^-/h^+) on its surfaces during photoreaction.[32] CdS suffers only the drawback of photocorrosion, that can be successfully suppressed by structural modification and metal cocatalysts.[33]

Metal sites serve as a co-catalyst when they exist in a semiconductor system (*e.g.*, CdS). They deliver multiple functions: (i) redox sites/active centres, (ii) surface plasmon effect, (iii) an extended optical response, (iv) suppressing charge recombination/back reactions by making Schottky junctions, (v) promoting electron transfer due to the alignment of the conduction band with the metal Fermi level.[34,35] The catalyst performance can be enhanced by the transfer of plasmonic electrons from metal Fermi levels to the surface of the semiconductor system, where hot electrons oscillate to achieve equilibrium for hydrogen liberation.[36]

Metals like Au, Ag, and Pd progressively contribute plasmonic oscillations that lead to localized electrons on the semiconductor system.[37,89] In recent years, attention has been aroused for a Cu/Pd system to induce plasmonic electrons on sunlight irradiation.[38] However, palladium contributes a relatively higher work function and generates surplus redox sites on CdS, whereas Cu contributes excess surface plasmon electrons.[39] It has been confirmed that the efficiency of the CdS system can be boosted *via* bimetallic cocatalysts that deliver a combined impact for a photocatalytic reaction.[40]

In order to harness the advantages of SPR supplementation and active sites, the current project was designed to develop a Cu–Pd/CdS catalyst system for hydrogen evolution. Successful synthesis of the catalysts has been achieved by a hydrothermal and chemical reduction approach. Higher hydrogen production activities are attributed to the synergy of SPR electrons contributed by copper and surplus redox sites generated by palladium cocatalysts. It is believed that Cu promotes SPR electrons that lead to an increase in electron density on CdS surfaces, while Pd cocatalysts suppress charge recombination *via* Schottky junctions.

Methodology

Chemicals

The chemicals used in this work are discussed in the ESI.†

Catalyst synthesis

To synthesize pristine CdS, an optimal concentration (35 mL) of $Cd(NO_3)_2$ (0.1 M) was transferred to a 100 mL 3-neck round-bottom flask. 17.5 mL of Na_2S (0.2 M) solution was added drop by drop to the above precursor. For optimal dispersion and homogeneity, the mixture was sonicated for 0.5 h. Note: to remove the dissolved oxygen, high-purity argon (Ar) gas was used as a purging agent before further treatment. This mixed solution was poured into an autoclave reactor for hydrothermal reactions at 160 °C for 5 h reaction time. After completion of the hydrothermal reaction, the product was sonicated for 30 minutes.[41] A yellow precipitate of pristine CdS was recovered *via* vacuum filtration. The precipitate was rinsed with deionized water and dried at 90 °C using a scientific oven (DHG-9030). Pristine CdS was ground into a fine powder and calcined at 350 °C. To prepare Cu–Pd/CdS catalysts, as-calcined CdS was used as a support. Catalysts with different metal ratios (*i.e.* $Cu_{0.2}$–$Pd_{0.8}$, $Cu_{0.4}$–$Pd_{0.6}$, $Cu_{0.6}$–$Pd_{0.4}$ and $Cu_{0.8}$–$Pd_{0.2}$) were successfully synthesized *via* chemical reduction. Typically, 250 mg of calcined CdS and 25 mL of distilled water were transferred into a 3-neck round-bottom reaction flask (RBRF). After 20 min of sonication, metal precursor solutions of Cu and Pd were added to the RBRF. After that, the reaction mixture was stirred for 2 h to ensure the homogeneous dispersion of metals in the CdS precursor. Metal ions were then reduced *via* super-cooled $NaBH_4$. The reduction of Cu/Pd metal ions was confirmed by a change in the color of the mixture (from yellow to black). To achieve maximum dispersion, the precipitate was then sonicated for 30 min. The catalysts, *i.e.* Cu–Pd/CdS, were thoroughly washed and recovered by vacuum filtration. To enhance surface rigidity and crystallinity, the catalysts were annealed at 410 °C. The as-prepared catalysts were preserved for characterization and photocatalytic reactions (Fig. 1).

Fig. 1 Schematic representation for the synthesis protocol of the catalysts.

Characterization

The techniques employed for characterization of the catalysts are discussed in the ESI.†

H_2 generation experiments

Hydrogen generation experiments were carried out in a reactor (quartz 140 mL; China). A broadband lamp equipped with UV cut-off filters and IR liquid filters was used to assess the wavelength-dependent performance. For each photoreaction, 6 mg of catalyst (the optimized amount) was dispersed in 50 mL of pure water. Note: prior to the photoreaction, the reaction mixture present in the reactor was purged with high-purity argon (Ar) to remove the dissolved oxygen content. Sunlight was used as an irradiation source. At different time intervals, a gas sample was extracted from the headspace of the reactor using a 0.5 mL syringe. The gas sample was then injected into a GC-TCD/Shimadzu-2014 installed with a molecular sieve capillary column. To achieve maximum accuracy, each photoreaction was repeated three times consecutively. The production rate of H_2 gas was calculated using the units mmol g^{-1} and mmol g^{-1} h^{-1}. The activities obtained for various catalysts, *i.e.*, CdS, Cu/CdS, Pd/CdS and Cu–Pd/CdS, are compared and discussed. The following equations have been used to calculate the quantum efficiencies:

$$\text{AQE}\,(\%) = \frac{2 \times \text{No. of } H_2 \text{ evolved}}{\text{No. of incident photons}} \times 100 \quad \text{(i)}$$

$$\text{AQE}\,(\%) = \frac{R_{H_2}(\text{mol s}^{-1}) \times t(\text{s}) \times 2}{N_A(\text{mol}^{-1}) \times n_p} \times 100 \quad \text{(ii)}$$

where, R_{H_2} is rate of H_2 production, t is total reaction time, N_A is Avogadro's number and n_p corresponds to the total number of photons. Sunlight with a photon flux approximately equal to 550 W m^{-2} was employed for the photoreaction. The number of photons was computed with the formula:

$$n_p = \frac{\text{Irr.}(\text{W cm}^{-2} = \text{J s}^{-1}\,\text{cm}^{-2}) \times \lambda(\text{m}) \times A(\text{cm}^2) \times t(\text{s})}{c(\text{ms}^{-1}) \times h(\text{J s})} \quad \text{(iii)}$$

where Irr. represents the incident source, λ is wavelength, A is the area of the reactor irradiated, c is the speed of light and h corresponds to Planck's constant.

Results and discussion

Structural assessment of catalysts

X-ray diffraction (XRD) analyses of pristine CdS, Cu/CdS, Pd/CdS and Cu–Pd/CdS catalysts were performed to determine their crystallinity and phase purity.

The XRD results of the aforementioned catalysts are represented in Fig. 2a. The results indicate that the XRD pattern of pristine CdS is well matched with JCPDS card no. 80-0019, confirming the high purity of the catalyst. Dominant peaks of CdS appear at 26.56°, 44.76°, 52.89° and 71.94°, corresponding to *hkl* values (111), (220), (311) and (331), respectively. The crystal structure of CdS has been confirmed as tetragonal, which is the preferred phase for photoreactions.[42] In the XRD pattern, two minor peaks of Cu metal were observed at 43.31° and 50.44°, corresponding to (111) and (200) *hkl* values, whereas peaks of Pd were perceived at 40.00° and 46.53°. It is worth mentioning that Cu and Pd exhibit quite low intensities. This is due to the low concentrations of metal content (0.2 to 0.8% overall). However, the presence of Cu and Pd was confirmed by the EDX and XPS studies.

To determine intermolecular bonding, FTIR analyses of all catalysts, *i.e.* pristine CdS, Cu/CdS, Pd/CdS and Cu–Pd/CdS catalysts, were performed and assessed. The results for all catalysts were found to be almost the same, and no change in intermolecular bonding was observed. See FTIR results in Fig. 2b. In the FTIR pattern, no distinct peaks of Cu and Pd were observed because of their extremely low percentage and physical attachment. A wide stretching vibration was observed at 517 cm^{-1} that corresponds to Cd and S bonding whereas bending vibration appeared at 1383 cm^{-1}. However, two major wide peaks observed at 1618 cm^{-1} and 3427 cm^{-1} correspond to the stretching and bending vibration of hydroxyl group of moisture content existing in the catalysts.[43]

Raman analyses of the catalysts were also performed to determine the vibrational modes of bonds developed between the constituents of the catalysts. Absorption peaks that appeared at 301 cm^{-1} and 602 cm^{-1} were attributed to 1LO and 2LO modes,[44] respectively. For clarification, see the results in

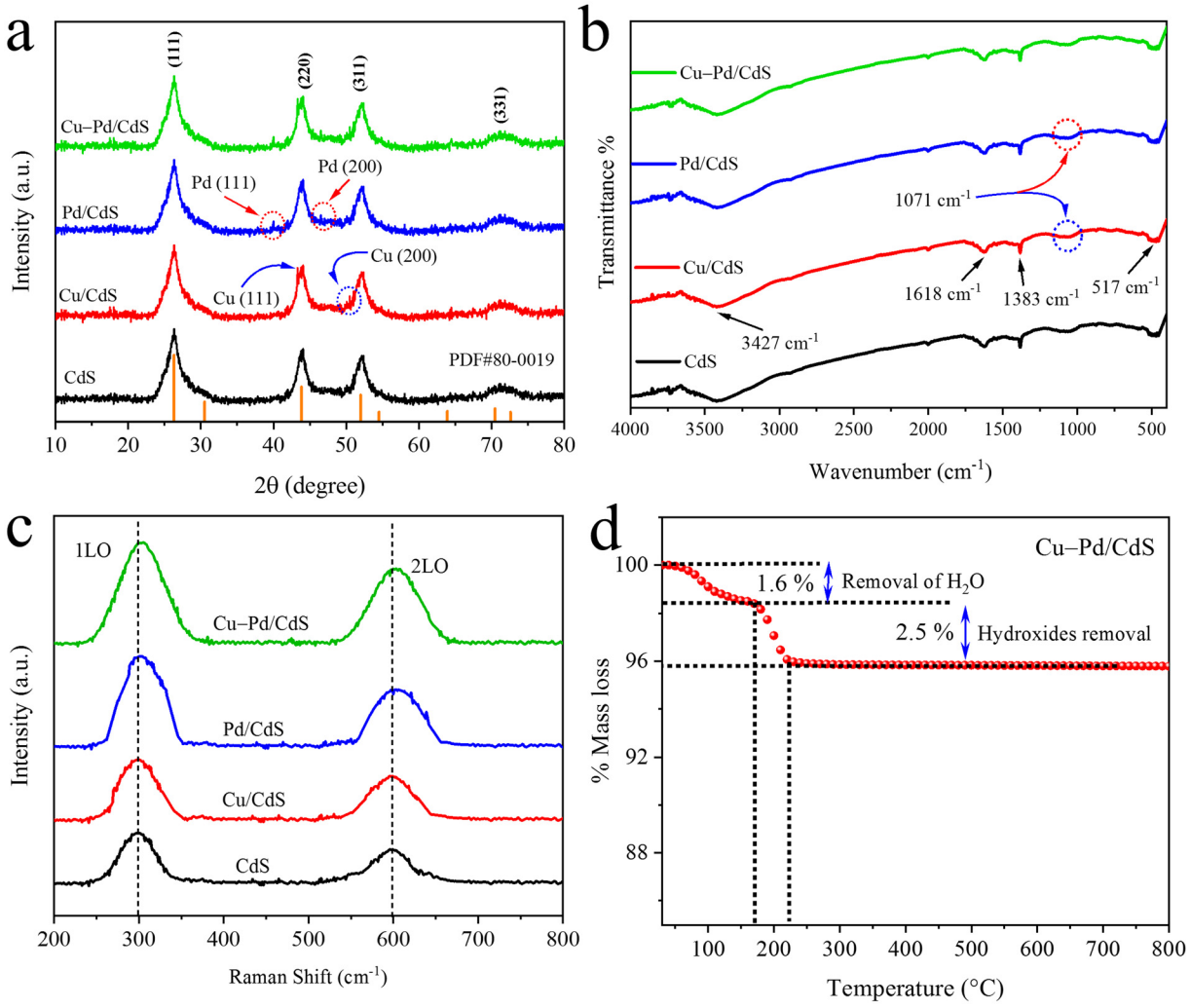

Fig. 2 (a) XRD patterns, (b) FTIR analyses, (c) Raman analyses and (d) TGA analysis of pristine Cu–Pd/CdS catalysts.

Fig. 2c. The results indicate that a slight red shift was observed due to the Pd metal phonon confinement effect.[45] The appearance of a red shift in the Raman analyses confirms the successful loading of Cu/Pd cocatalysts over CdS surfaces.[46]

Thermogravimetric analysis of Cu–Pd/CdS catalysts was performed to check the thermal stability of the catalysts. A gradual decrease in mass was observed due to the increase in temperature. However, out of 4.1% overall loss, 1.6% loss of mass is due to removal of moisture content (see Fig. 2d), whereas 2.5% decrease in mass is due to removal of oxides.[47] Beyond 225 °C, there was no further loss in the mass of the catalysts, confirming their stability.

Confirmation of surface morphology

The morphology of the Cu–Pd/CdS catalysts was determined by scanning electron microscopy (SEM) with an EDX accessory and high resolution transmission electron microscopy (HRTEM).[48] SEM images of Cu–Pd/CdS catalysts are illustrated in Fig. 3(a and b) that reveal a tetragonal morphology along with the presence of some voids. Upon careful examination, some stacked CdS particles were noticed in the image at 1 μm. For clarification, see the results in Fig. 3a. The results confirmed that tetragonal particles of CdS were piled on each other; hence they appeared stacked. In the stacked structures, the presence of voids or gaps accommodate the photo-induced charges involved in hydrogen evolution reactions.[49] To investigate the existence of Cu and Pd, HRTEM analysis was performed and it was confirmed. See the results in Fig. 3(c & d). In the HRTEM images, crossed lattice fringes confirm the crystalline planes (111) of Pd and (110) of Cu on CdS. The interplanar spacings (*d* spacing) were measured by Bragg's law to be 0.36 nm, 0.22 nm and 0.205 nm for CdS, Pd and Cu, respectively.[50] EDX analysis emphasized the elemental composition. All essential elements of the catalysts, *i.e.* Cd, S, Cu, and Pd, have been detected in the EDX spectrum; see Fig. 3e. Confirmation of the presence of Cu and Pd cocatalysts anticipated the successful synthesis and novelty of the work.

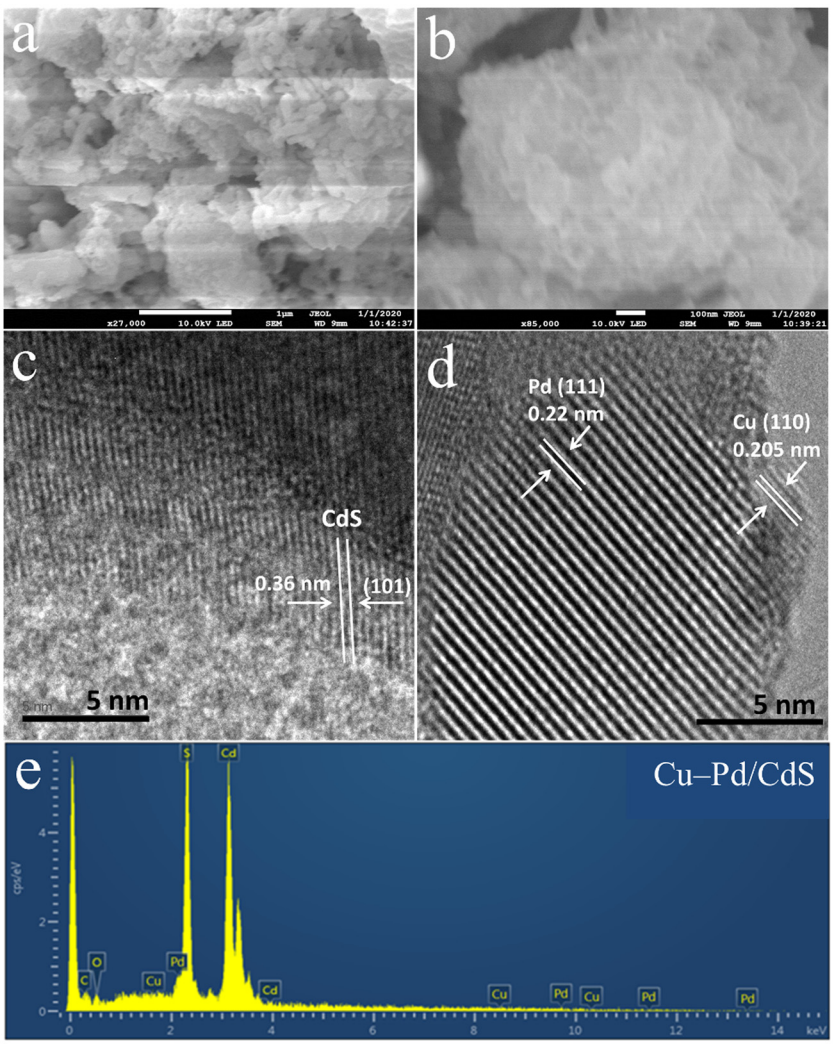

Fig. 3 Scanning electron microscopic images of catalysts: (a) 1 μm image, (b) 100 nm image. (c & d) HRTEM images and (e) EDX analysis of Cu–Pd/CdS catalysts.

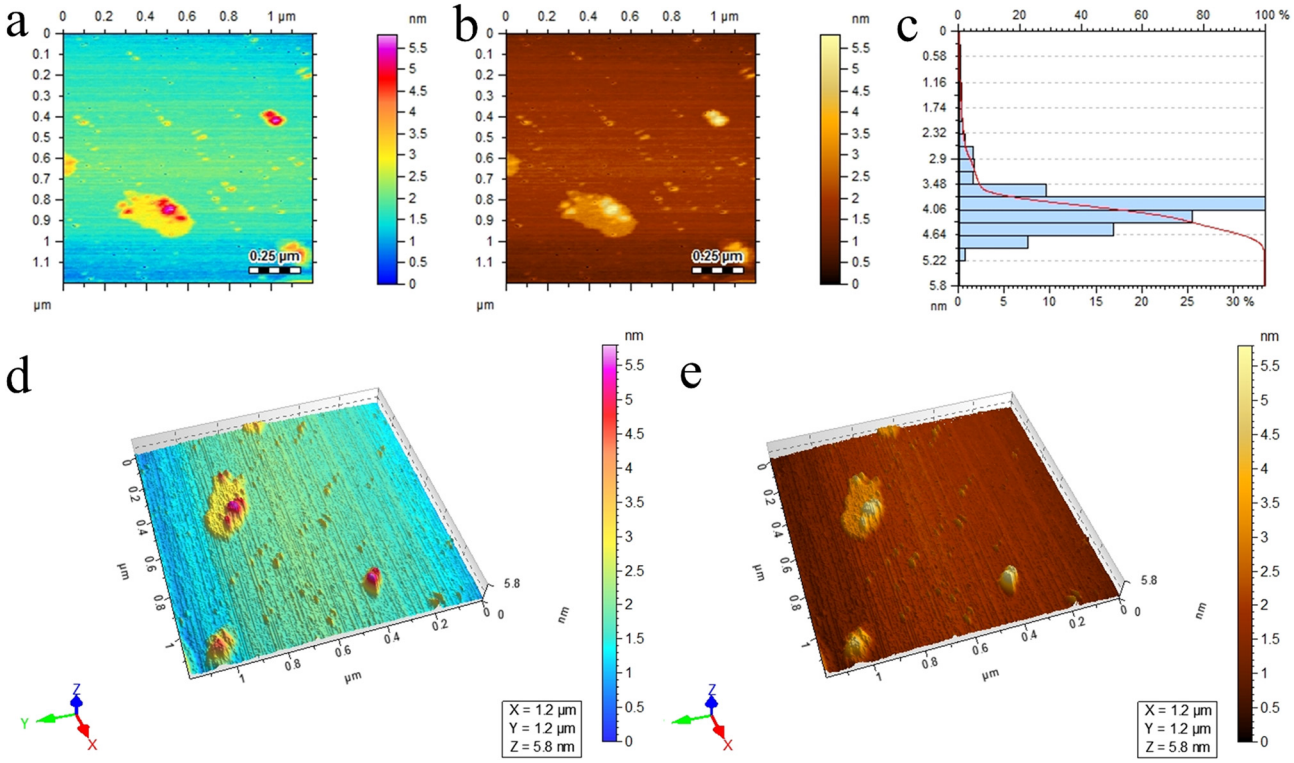

Fig. 4 AFM images: (a and b) 2D images, (c) height scale, (d & e) 3D images of Cu–Pd/CdS catalysts.

Confirmation of required surfaces and topography

Atomic force microscopy (AFM) is a wonderful analytical technique that is commonly used to determine the surface properties of catalysts.[51] AFM was employed to assess the surface properties of the Cu–Pd/CdS catalysts. Fig. 4(a and b) represent 2D images of the catalyst surface. The results revealed that Cu and Pd particles are widely dispersed on the smooth planes/surfaces of CdS. The height scale was used to measure the elevation and it was found that the average height of the catalysts was 4.06 nm. See the results in Fig. 4c. To confirm the height, length and surface area, 3D images of the catalysts were also assessed and discussed. For the results, see Fig. 4(d & e).

Assessment of composition and oxidation states

The composition and chemical states of the elements present in Cu–Pd/CdS were investigated by X-ray photon spectroscopy (XPS), and the results obtained from the XPS analysis of the catalysts are shown in Fig. 5(a–e). All essential elements of the catalysts were detected in the XPS survey scan spectrum.[52] Cd and S were detected in the survey scan spectrum as a semiconductor, where Cu and Pd exist as cocatalysts. See Fig. 5a. The results reveal that Cu 2p showed two binding energies, *i.e.*, 933.07 eV and 952.47 eV, corresponding to Cu $2p_{3/2}$ and Cu $2p_{1/2}$, respectively, indicating copper in both metallic and oxidized states.[16,53] See the results in Fig. 5b. Similarly, the XPS spectrum of Pd presented in Fig. 5c revealed two peaks at binding energies of 335.67 eV and 340.87 eV assigned to the characteristic states of Pd $3d_{5/2}$ and Pd $3d_{3/2}$, respectively. It is worth mentioning that Pd exists in the metallic state (*i.e.* Pd^0), which is quite important for quenching electrons for water reduction.[54] Fig. 5d presents the XPS spectrum of Cd, where two major multiples were observed at 405.07 eV and 411.87 eV, agreeing with Cd $3d_{5/2}$ and Cd $3d_{3/2}$, respectively. The binding energy of Cd suggests that it exists in the divalent state (Cd^{2+}). The XPS spectrum of S is shown in Fig. 5e, exhibiting the characteristic binding energies of S $2p_{3/2}$ and S $2p_{1/2}$ at 160.97 eV & 162.27 eV, respectively. The results revealed that sulfur exists in the S^{2-} oxidation state.

Assessment of optical properties

The ultraviolet diffuse reflectance spectra of pristine CdS, Cu/CdS, Pd/CdS and Cu–Pd/CdS catalysts are illustrated in Fig. 6a. Remarkably, these catalysts exhibit similar absorption profiles with a step absorption edge in visible range that corresponds to the band gap energy of the catalysts. Comparative analysis indicates that CdS exhibits absorption in the visible range of the solar spectrum, *i.e.*, 540 nm, whereas Cu–Pd/CdS catalysts exhibit extended absorption at 548 nm. Cu/CdS and Pd/CdS absorption lies in the 540–548 nm range of the visible region. The bandgap energy of the catalysts was calculated using the Tauc plot method (Fig. S2†). Thus, the UV-Vis/DRS results confirmed that the extended absorption and decreased bandgap energy (from 2.42 to 2.39 eV) are due to the presence of Cu and Pd cocatalysts.[55] It is believed that the extra absorption around 600 nm is due to the SPR impact of the cocatalysts. This SPR effect was confirmed by wavelength-dependent experiments (Fig. S5†).[56]

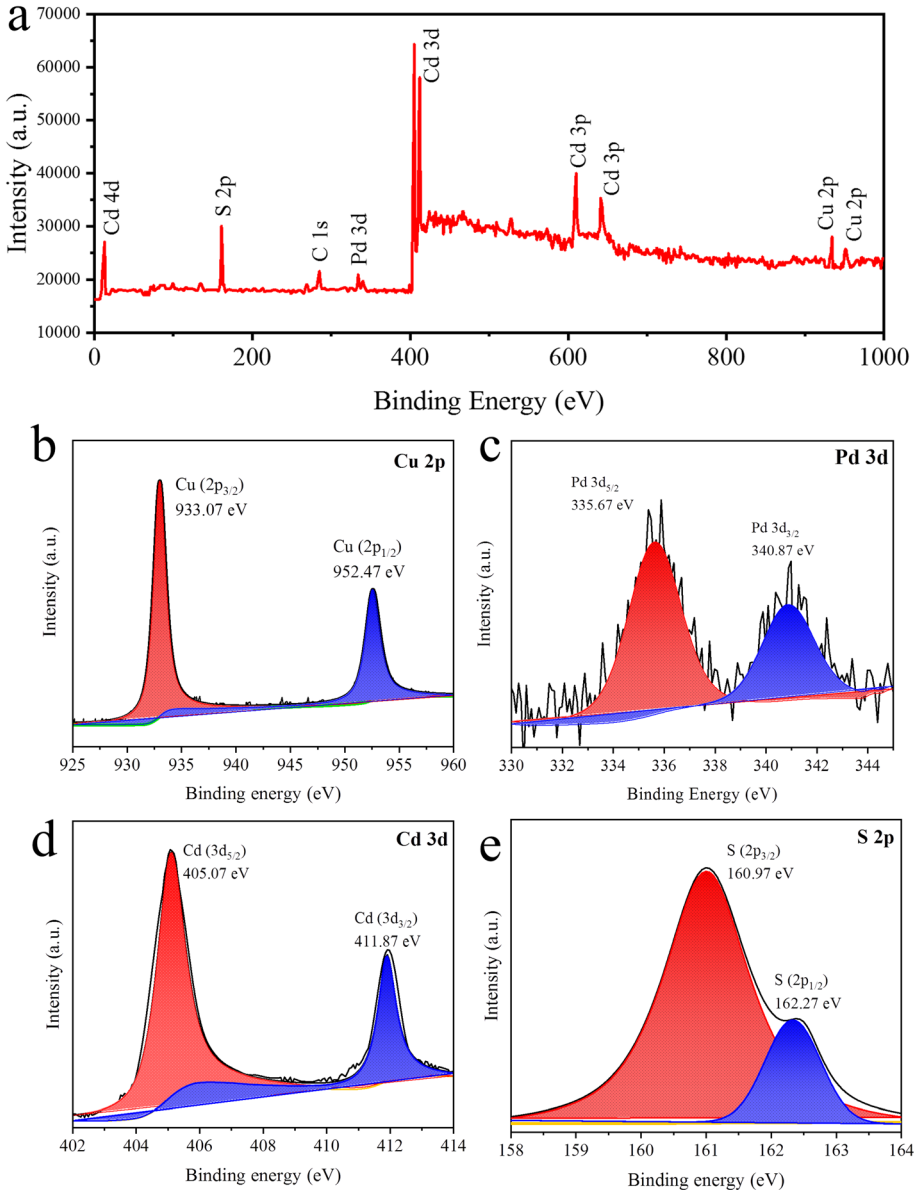

Fig. 5 XPS results: (a) XPS survey scan, (b) Cu 2p spectrum, (c) Pd 3d spectrum, (d) Cd 3d spectrum and (e) rS 2p spectrum.

Photoluminescence studies were performed to evaluate the charge recombination and charge transfer rates. The PL results of CdS, Cu/CdS, Pd/CdS and Cu–Pd/CdS catalysts are illustrated in Fig. 6b. The results indicated that CdS exhibits high-intensity PL emission due to fast recombination of photogenerated charges.[57] However, the Pd/CdS catalysts exhibit lower intensity PL emission than pristine CdS, because Pd metal creates a Schottky barrier that acts as rectifying points on the semiconductor system to suppress the recombination of charges. The as-synthesized Cu–Pd/CdS catalysts exhibit the lowest PL emission, confirming higher transfer to the active sites.[58] The rate of photogenerated charge recombination, defects/traps, and charge transfer in CdS, Cu/CdS, Pd/CdS and Cu–Pd/CdS catalysts was assessed using the TRPL technique. The obtained results (Fig. S3†) illustrate effective charge transfer from CdS to the Cu and Pd cocatalysts. The lifetime of the Cu–Pd/CdS catalysts (4.1 ns), is significantly higher than that of pure CdS (0.6 ns) or monometallic catalysts.[57]

Furthermore, to evaluate the interface charge transfer resistance of the semiconductor, electron impedance spectroscopic (EIS) analysis was performed. Resistance to the transfer of charges can be determined by the arc radius of EIS analysis; see the EIS results in Fig. 6c. Pristine CdS exhibits a large arc radius that means resistance to the transfer of charges is high. Cu–Pd/CdS catalysts exhibit a lower arc radius than the other catalysts in this work. This is evidence that resistance to the transfer of charges is minimum, emphasizing more charge transfer to the active sites.[59] Moreover, photocurrent studies were also carried out to reassess the separation and transfer of

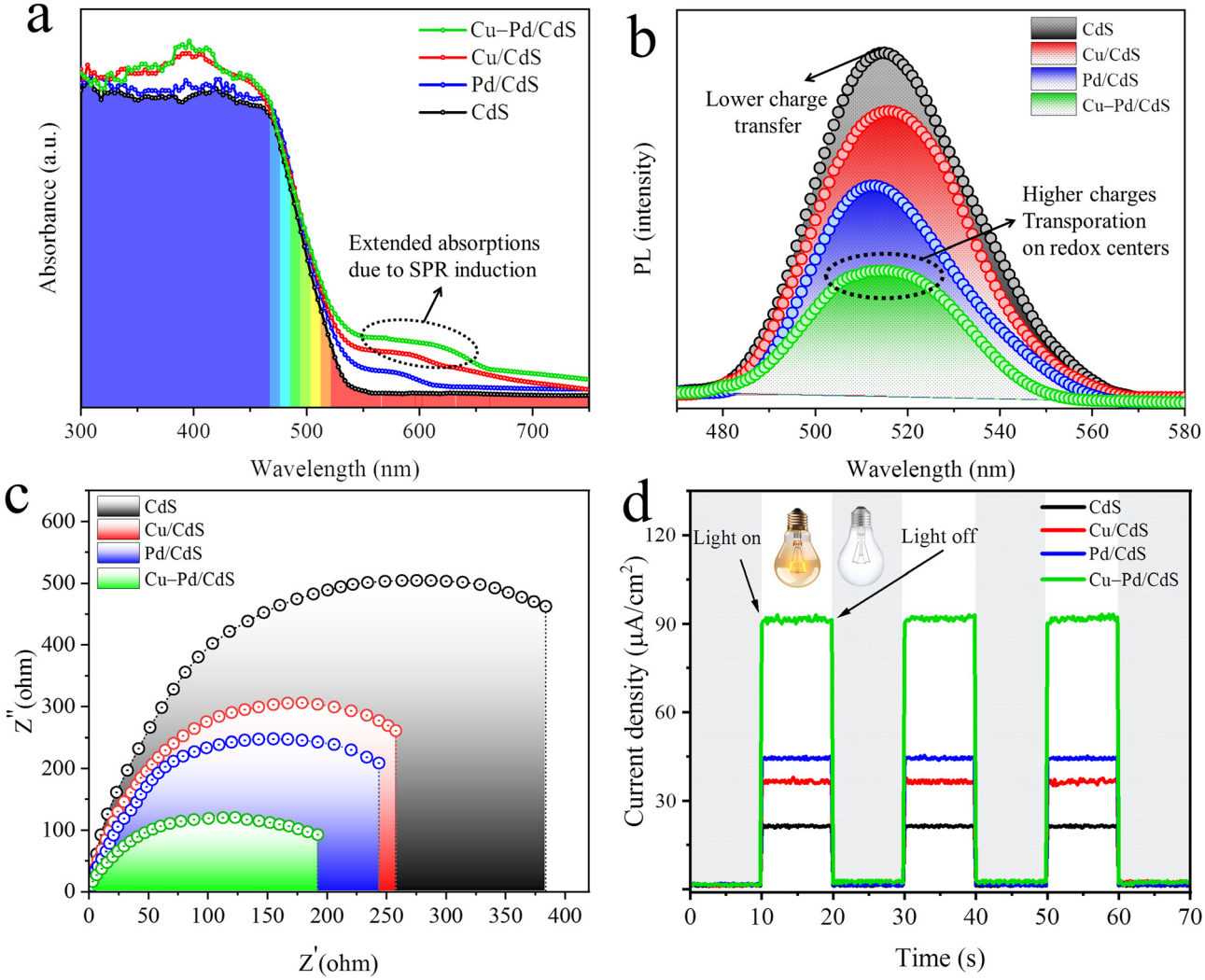

Fig. 6 (a) UV-Vis/DRS spectrum, (b) PL analysis, (c) EIS measurements and (d) photocurrent analysis of the catalysts.

these charges. Fig. 6d illustrates the photocurrent responses of the catalysts with light on/off cycles. The results indicate that CdS exhibits the lowest current density response compared to the other catalysts.[59] Whereas the Cu–Pd/CdS catalysts exhibit a high current density response that ensures relatively more charges transfer on active centres, which is the main reason for their excellent activities.

The Mott–Schottky approach was used to determine the locations of the CBs of the Cu–Pd/CdS and CdS catalysts (Fig. S4†). The obtained results show the CB potential of CdS was around −0.72 eV, while that of Cu–Pd/CdS was approximately −0.81 eV. The valence band locations were determined using UV-VIS/DRS and eqn (iv):[60]

$$E_{VB} = E_{CB} + E_G \quad \text{(iv)}$$

The VB and CB potentials are denoted by E_{VB} and E_{CB}, respectively. The Cu–Pd/CdS and CdS catalysts were found to have E_{VB} values of 1.58 and 1.70 eV, respectively.

Assessment of H_2 production activities

The hydrogen generation activities of all the synthesized catalysts, pristine CdS, Cu/CdS, Pd/CdS and Cu–Pd/CdS, were assessed and are presented in Fig. 7(a and b) and Table 1. It is important to declare that the photoreactions for each catalyst were carried out for 6 h and 6 mg of each catalyst was the optimized amount for the photoreaction. Comparative catalytic H_2 generation activities were evaluated for pristine CdS, Cu/CdS, Pd/CdS and Cu–Pd/CdS catalysts. Comparative activities are exhibited in Table 1. It is worth mentioning that no hydrogen evolution was observed in the absence of light or catalyst. However, the photoreaction of pristine CdS delivers 4.41 mmol g^{-1} h^{-1} of hydrogen. The low yield of hydrogen for pristine CdS is due to higher charge recombination and catalyst decomposition.[61] Note: The individual impacts of Cu and Pd cocatalysts were evaluated. Various concentrations of % Cu and % Pd on CdS were utilised to evaluate the optimised concentration. It was observed that $Cu_{1.0}$/CdS and $Pd_{1.0}$/CdS

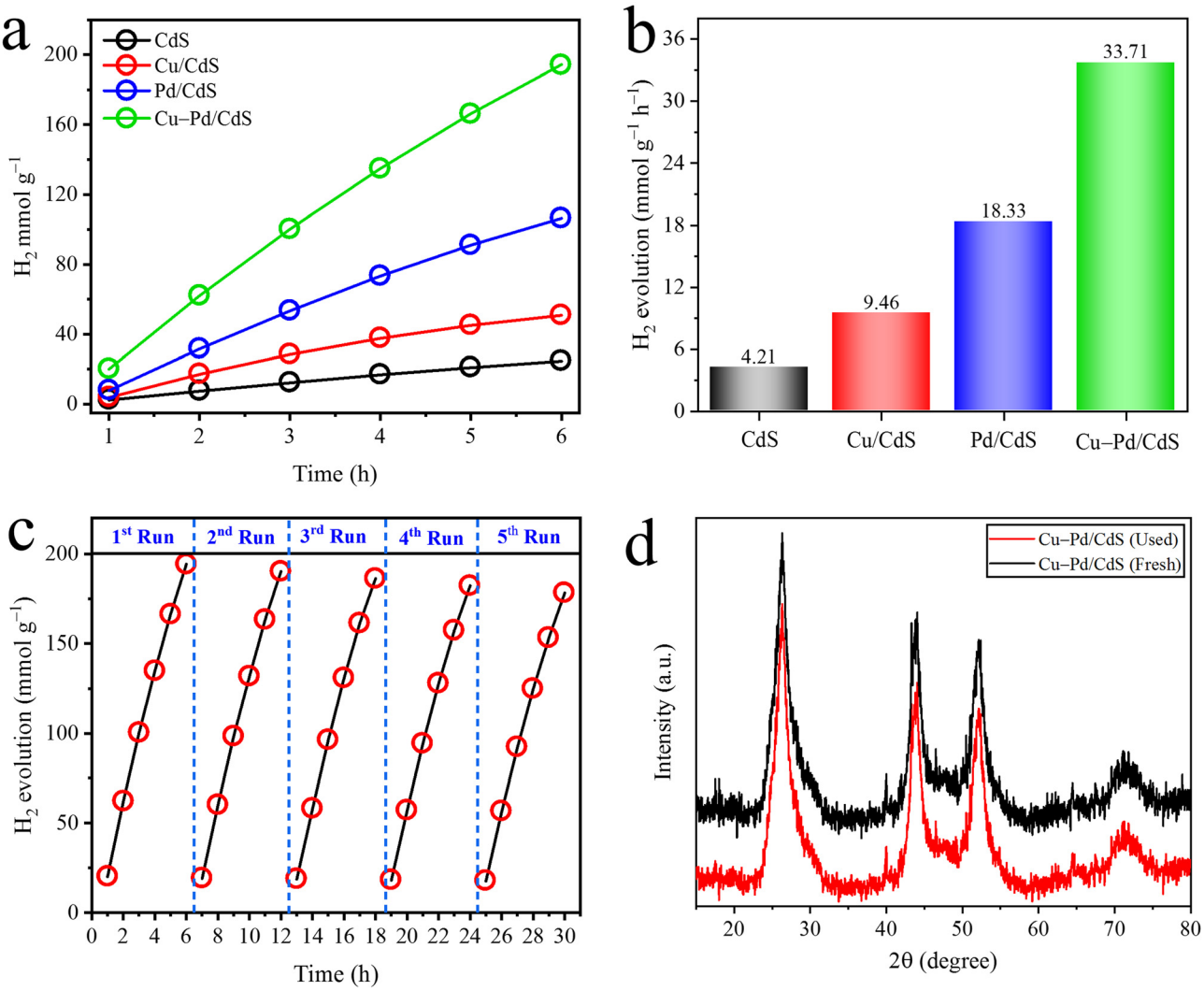

Fig. 7 H_2 evolution activities: (a) overall H_2 evolution (mmol g^{-1}), (b) H_2 evolution (mmol g^{-1} h^{-1}), (c) recyclability test of catalysts and (d) XRD results of fresh and used catalysts.

Table 1 Comparison of H_2 production rates of all photocatalysts

Sr. no.	Catalyst[a]	wt% of Cu : Pd	H_2 production		Q.E (%)
			mmol g^{-1}	mmol g^{-1} h^{-1}	
1	CdS	0.0 : 0.0	24.62	4.21	4.2
2	Cu/CdS	1.0 : 0.0	50.81	9.46	9.6
3	Pd/CdS	0.0 : 1.0	106.42	18.33	18.5
4	Cu–Pd/CdS	0.2 : 0.8	194.32	33.71	34.3

[a] 6 mg of catalyst was used for each photoreaction.

deliver hydrogen at 9.46 mmol g^{-1} h^{-1} and 18.33 mmol g^{-1} h^{-1}; the results are illustrated in Fig. S6 and S7,† respectively. The activities clearly indicate that the $Pd_{1.0}$/CdS catalyst delivers more hydrogen than the $Cu_{1.0}$/CdS system. The reason is that Pd creates a Schottky junction and contributes a higher work function to promote fast electron transfer on active sites. Whereas Cu exhibits a relatively low work function that is not very effective for charge transfer.[16] However, the role of Cu becomes significant when it works alongside Pd cocatalysts, because Cu contributes inherent SPR electrons that ensure an extra supply of electrons at the semiconductor surface. To cope the combined advanaged of Cu and Pd cocatalysts, Pd, Cu–Pd/CdS catalysts were synthesised and assessed for hydrogen evolution experiments. However, wavelength-dependent activities were employed to confirm the role of SPR electrons for hydrogen evolution; see the results in Fig. S5.† It is quite important to indicate the loading of cocatalysts: *i.e.*, Cu/Pd was fixed up to 1.0% overall on CdS surfaces. Catalysts with various Cu to Pd ratios, *i.e.*, $Cu_{0.8}$–$Pd_{0.2}$/CdS, $Cu_{0.6}$–$Pd_{0.4}$/CdS, $Cu_{0.4}$–$Pd_{0.6}$/CdS, and $Cu_{0.2}$–$Pd_{0.8}$/CdS, were evaluated (Fig. S8†) to predict the ideal ratio (*i.e.*, optimized amounts). The activities indicated that among them, $Cu_{0.2}$–$Pd_{0.8}$/CdS was the most active catalyst of the series, potentially delivering 33.71 mmol g^{-1} h^{-1} of hydrogen. The study emphasized that catalysts with higher Cu contents relative to Pd were less effective, because the

Table 2 Comparison of H_2 evolution with recent reports

Catalyst	Light source	Catalyst amount (mg)	Sacrificial reagent	H_2 mmol g^{-1} h^{-1}	Ref.
Cu–Pd/CdS	Sunlight	6	—	33.71	This study
Au-BaO@TiO_2/CdS	Xe lamp	10	—	13.54	64
Au@TiO_2/CdS	Hg lamp	10	Ethanol	19.15	65
CDs/CdS	Sunlight	40	Lactic acid	6.70	66
Cu/Ni@CdS	Sunlight	5	Ethanol	14.16	16
$CdCO_3$/CdS	Xe lamp	—	—	1.93	67
Cu/Ag@CdS	Sunlight	5	Ethanol	18.93	53
Ni doped CdS	Xe lamp	4	Ethanol	3.86	68
CdS@a-CN	Xe lamp	10	Na_2S/Na_2SO_3	0.244	69
Ni/S@CdS	Xe lamp	10	Na_2S/Na_2SO_3	2.56	70

higher amount causes a shadowing effect (*i.e.*, less penetration of photons on the CdS surface).[16,62] However, by increasing the Pd content, the rate of hydrogen production is enhanced, confirming the electron quenching ability of Pd cocatalysts.[63] Table 2 shows the comparative activities of the current work with reported studies.

Recyclability experiment

Cyclic experiments were performed to assess the reusability and stability of Cu–Pd/CdS. Five consecutive experiments were carried out to confirm the stability of the catalysts. These experiments were conducted under 550 W m^{-2} light intensity. The pH was adjusted to 10, and 6 mg of catalyst was used in 50 mL of water. The temperature of the reaction mixture was maintained at 55 °C. The results of the recyclability test are presented in Fig. 7c.

In the first run of the recyclability test, the catalysts deliver the highest amount of hydrogen. However, when it was applied for the fourth and fifth runs, a minor decrease in the hydrogen production rate was observed. The decrease in activity was attributed to the loss of catalyst particles during the washing and recovery process.[71] Thus, cyclic experiments confirm that the catalysts sustain their stability during the photoreaction and can be reused after proper recovery. Furthermore, XRD and SEM analyses of the used catalysts were performed to confirm the structural, morphological and chemical stability of the catalysts. The XRD results revealed that after photoreaction, the catalysts maintained their stability, because no significant alteration in the XRD patterns of the used catalysts was witnessed (see Fig. 7d). The SEM results (Fig. S1†) confirmed the stable morphology of the catalysts.

Photocatalytic water splitting mechanism

Although water is a stable molecule and it requires 237 kJ mol^{-1} of Gibbs free energy to completely split into its constituents, its activation energy can be progressively decreased using efficient catalysts. Thus photocatalytic water splitting has become a promising approach to harvesting green and renewable energy.[72] Unfortunately, in the last few decades, this technology has not received proper attention from investors. Another reason is that some international organizations, OPEC, GECF, IEA *etc.*, seem not to be serious due to financial constraints.[65,73] It is worth mentioning that the water splitting reaction is completed in two half reactions: *i.e.*, oxidation requiring 1.23 eV, and reduction that occurs at zero electrode potential.[74] Current work indicates that Cu–Pd/CdS catalysts are stable and quite efficient for splitting water on sunlight irradiation. The described catalysts exhibit several characteristics, such as (i) excellent band potentials, (ii) stability for recyclability, (iii) the contribution of SPR to supplying extra electrons, (iv) a Schottky junction that promotes the transfer of charges on active centres, (v) extended absorption in visible light.[69] Upon exposure to sunlight, Cu starts to induce SPR electrons on the semiconductor surface (*i.e.*, CdS), whereas Pd metal develops a Schottky junctions that rectifies the SPR electrons to reinforce water reduction. Due to its higher work function, Pd can progressively quench the electrons to promote charge transfer on active sites.[16,75] It is worth mentioning that electrons flow from a material with a low work function to one with a higher work function. The work functions of the CdS catalysts have been calculated utilizing UPS with a helium discharge lamp with a photon energy of 21.21 eV and the cut-off energy was measured to be 16.13 eV (Fig. S9†). The work function (Φ) was calculated using eqn (v),[76] and is 5.08 eV:

$$\Phi = h\nu - K \cdot E_{\max} \quad \text{(v)}$$

The work functions of Cu (4.7 eV) and Pd (5.3 eV) are well defined and reported. The lower work functions of Pd and CdS suggest that the electrons flow from Cu to CdS and then towards Pd (*i.e.*, active sites). The difference in work functions of Cu and Pd cocatalysts, contribute to the formation of Schottky junctions. During photoreaction, H^+ is readily reduced to hydrogen atoms that simultaneously react with each other to produce H_2 molecules.[77]

Fig. 8 represents the mechanistic approach for water splitting in the presence of sunlight. It can clearly be seen that Cu metal transfers its SPR charges to the surfaces, whereas Pd quenches these electrons by rectification with Schottky barriers. It is believed that due to presence of Cu/Pd, the Fermi level of CdS is altered during the photoreaction and gets shifted into the new potential to attain equilibrium.[70]

On the other hand, it is essential to utilize holes (h^+) present on valence bands to restrict the back reaction.[78] In the current work, holes were consumed by the hydroxyl ions (OH^-)

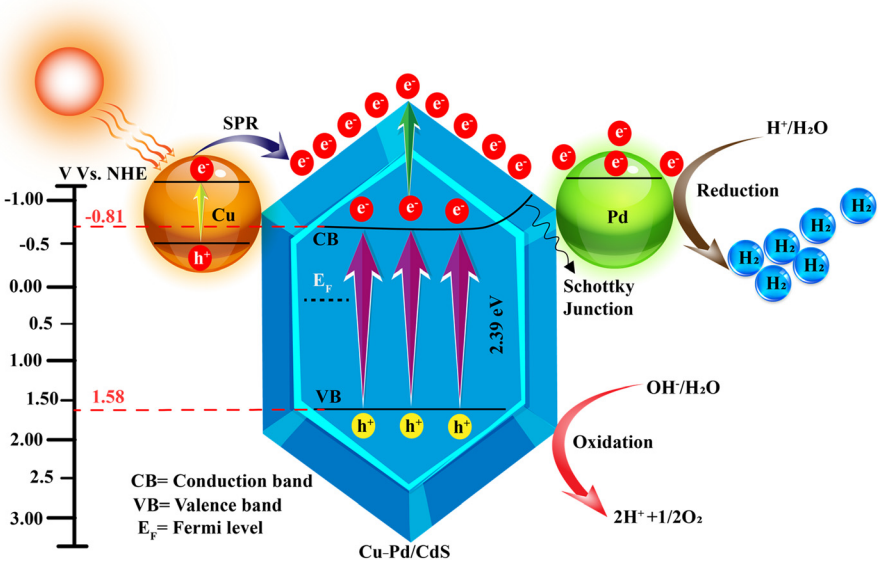

Fig. 8 Photocatalytic water splitting mechanism for H_2 evolution.

produced during water oxidation. When hydroxyl ions react with holes, they are readily converted into hydroxyl radicals: *i.e.*, $^{\bullet}OH$. These radicals further react with H^+ to promote redox reactions.[79] Here is a scheme that demonstrates the reactions involved in the photoreaction:

$$Cu - Pd/CdS + h\nu \xrightarrow{h\nu \geq 2.4\,eV} (VB)\,h^+ + (CB)\,e^- \quad \text{(vi)}$$

$$\text{Photocatalyst} + H_2O \rightarrow H^+ + OH^- \quad \Delta G^\circ = 237.2\ \text{kJ mol}^{-1} \quad \text{(vii)}$$

$$(CB)\ 2e^- + 2H^+ \rightarrow H_2\ \text{(Reduction reaction)} \quad E = 0.0\ \text{eV} \quad \text{(viii)}$$

$$(VB)\ h^+ + OH^- \rightarrow (^{\bullet}OH)\ \text{(Oxidation reaction)} \quad E_0 = 1.23\ \text{eV} \quad \text{(ix)}$$

where CB and VB represent conduction and valence band, respectively.

Factors influencing the rate of H_2 production

The activity or catalytic progress of hydrogen production can be affected by several factors. In this study, we investigated the effect of pH, temperature, catalyst dose and the intensity of light for the photocatalytic hydrogen generation on Cu–Pd/CdS.

pH

The pH of the reaction mixture has a considerable impact on the photocatalytic hydrogen evolution rate. In this study, hydrogen evolution experiments were carried out at different pH values: pH values from 4 to 12 were used in the presence of most active Cu–Pd/CdS catalysts. The maximum hydrogen evolution rate was observed in basic medium. At pH 10, the activity of the catalysts was 33.10 mmol g^{-1} h^{-1}, as shown in Fig. 9a and Table S1.† At high pH, more ^{-}OH ions were present and served as hole scavengers to promote the transfer of electrons for reduction reactions at the surface of the catalysts.[80] The results show that the stability of the photocatalysts was reduced in both acidic and basic media, resulting in a decrease in the hydrogen evolution rate.[81]

Temperature

Temperature variation normally does not have a substantial impact on the production of hydrogen thermodynamically.[82] However, it was noticed that temperature has an incredible effect on the adsorption and desorption of hydrogen at the surface of the photocatalysts. Temperature can alter the overall effectiveness of the catalytic process by altering the adsorption and desorption of hydrogen on the catalyst surfaces, even it is thermodynamically impossible to induce electrons for hydrogen creation.[83] It was observed that, as we increased the temperature, the rate of hydrogen production also increased gradually, because with the increase in temperature, desorption of hydrogen gas increased from the catalyst surface. High temperatures promote the formation of charges and facilitate the transfer of electrons from the valence band to the conduction band of the semiconductor. Extremely high temperatures can lead to an increase in the vapor pressure of the reaction mixture, which results in a decrease in the efficiency of the photoreaction.[84] It was observed that a temperature of 55 °C and pH of 10 of the reaction mixture are ideal for hydrogen evolution. Under these conditions, the rate of hydrogen evolution was observed to be 33.17 mmol g^{-1} h^{-1} over most active Cu–Pd/CdS catalysts; see Fig. 9b and Table S2.† These studies demonstrate that optimization of these factors maximizes the activity of the catalysts for hydrogen production.

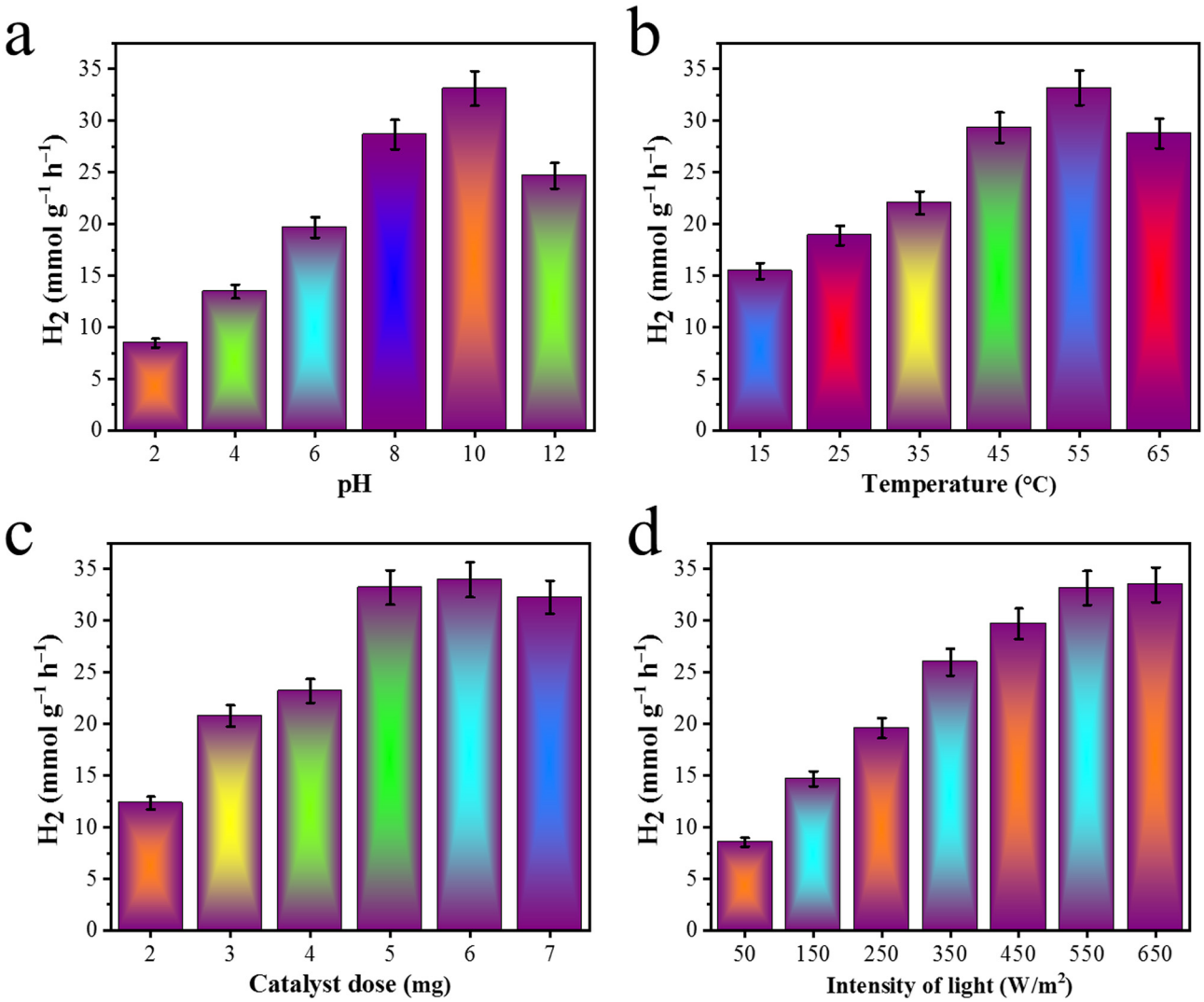

Fig. 9 Factors influencing the rate of H_2 production: (a) pH, (b) temperature, (c) catalyst dose, and (d) light intensity.

Photocatalyst dose

The rate of hydrogen production was also significantly influenced by the concentration of photocatalyst.[85] In this work, 2–7 mg doses of Cu–Pd/CdS photocatalyst were used in a 150 mL Pyrex reactor to evaluate the effect of photocatalyst concentration on the activity of the catalyst. It was observed that, as the catalyst concentration was increased to 5 mg, the rate of H_2 production increased because more photogenerated charges were available. However, beyond a specific concentration of photocatalyst *i.e.* 5 mg, further additions did not considerably improve the activity of the catalyst for hydrogen production.[86] The reduction in activity was attributable to less exposure of the catalyst surface to light due to aggregation of catalyst particles. A higher photocatalyst concentration caused particle build-up, which reduced the exposure of light to the active sites of the catalysts.[87] The highest hydrogen production was observed under optimized pH and temperature conditions (pH = 10, temperature = 55 °C) with an optimized photocatalyst dosage of 5 mg, and was 33.19 mmol g^{-1} h^{-1}; see Fig. 9c and Table S3.†

Intensity of light

It was observed that increasing the light intensity of the light source increases the rate of hydrogen production from the water splitting reaction.[73] Fig. 9d and Table S4† demonstrate that under light exposure of 550 W m^{-2}, 33.14 mmol g^{-1} h^{-1} of hydrogen was produced using Cu–Pd/CdS catalysts. This shows that the catalyst was already generating the greatest amount of charge during the photoreaction at this particular light intensity (550 W m^{-2}), leading to the highest rate of hydrogen production. Beyond this limit, however, an increase in light intensity had no discernible effect on the catalyst activity. This means that the catalyst had achieved its saturation point, and was producing charges for efficient hydrogen generation.[88]

Conclusions

In the current project, Cu/CdS, Pd/CdS and Cu–Pd/CdS catalysts have been successfully prepared and assessed for catalytic H_2 production on sunlight irradiation. All the catalysts were synthesized by a hydrothermal and chemical reduction approach under similar conditions. To extend their activity and effectivity, the CdS surfaces were decorated with Cu and Pd cocatalysts. The structural and surface morphology of catalysts was assessed *via* FTIR, XRD, Raman, SEM, HRTEM and AFM analytical techniques. Optical characteristics and electrons transfer studies were evaluated by UV-Vis/DRS, EIS, PL and photocurrent analyses, whereas the elemental composition and purity of the catalysts were confirmed by XPS and EDX approaches. Photocatalytic activities revealed that $Cu_{0.2}$/$Pd_{0.8}$@CdS is the most active catalyst, potentially delivering 33.71 mmol g^{-1} h^{-1} of H_2, which is higher than the activity of pristine CdS, Cu/CdS or Pd/CdS. Higher activities were attributed to the combined impact of Cu and Pd cocatalysts. Cu cocatalysts induce SPR electrons, whereas Pd makes Schottky junctions on CdS surfaces. Schottky junctions facilitate the rectification of the transfer of electrons to the active sites. Pd cocatalysts progressively quench the electrons from the surfaces to be utilized for water reduction reactions. Additionally, Schottky junctions effectively suppress charge recombination (back reaction) by rectifying the charges onto active sites. On the basis of the results and activities, it has been concluded that the as-synthesised catalysts hold promise for the eventual transition to renewable hydrogen technologies.

Data availability

The data and necessary protocols of this study have been included as part of the ESI.†

Conflicts of interest

There are no conflicts to declare.

Acknowledgements

The project was sponsored by HEC of Pakistan under grant no. 377/IPFP–II (Batch–I) SRGP/NAHE/HEC/2020/27. Current work accredited to the Inorganic Material Laboratory (52S), Institute of Chemistry, The Islamia University of Bahawalpur. Dr Ejaz Hussain thanks Ministry of Science and Technology of Pakistan (Renewable Energy Sector), Carnegie Mellon University (CMU) of USA, and University of Karachi (HEJ–center) for characterizations and scientific support. Moreover, this study is supported *via* funding from Prince Sattam Bin Abdulaziz University project no. PSAU/2024/R/1445.

References

1 I. Capellán-Pérez, M. Mediavilla, C. de Castro, Ó. Carpintero and L. J. Miguel, *Energy*, 2014, **77**, 641–666.
2 D. J. Wuebbles and A. K. Jain, *Fuel Process. Technol.*, 2001, **71**, 99–119.
3 A. Boretti, *Int. J. Hydrogen Energy*, 2024, **51**, 8–17.
4 A. Hosseinzadeh, J. L. Zhou, X. Li, M. Afsari and A. Altaee, *Renewable Sustainable Energy Rev.*, 2022, **156**, 111991.
5 S. E. Hosseini and M. A. Wahid, *Renewable Sustainable Energy Rev.*, 2016, **57**, 850–866.
6 A. Z. Naser, I. Deiab and B. M. Darras, *RSC Adv.*, 2021, **11**, 17151–17196.
7 A. Fujishima and K. Honda, *Nature*, 1972, **238**, 37–38.
8 U. Congress, *US public law* 102-486, 1992.
9 A. Pareek, R. Dom, J. Gupta, J. Chandran, V. Adepu and P. H. Borse, *Mater. Sci. Energy Technol.*, 2020, **3**, 319–327.
10 I. Jain, *Int. J. Hydrogen Energy*, 2009, **34**, 7368–7378.
11 P. J. Megía, A. J. Vizcaíno, J. A. Calles and A. Carrero, *Energy Fuels*, 2021, **35**, 16403–16415.
12 N. Sazali, *Int. J. Hydrogen Energy*, 2020, **45**, 18753–18771.
13 P. Nikolaidis and A. Poullikkas, *Renewable Sustainable Energy Rev.*, 2017, **67**, 597–611.
14 M. Jalil, K. Rafiq, M. Z. Abid, M. Rafay, A. Rauf, R. Jin and E. Hussain, *Catal. Sci. Technol.*, 2024, **14**, 850–862.
15 M. Z. Abid, A. Tanveer, K. Rafiq, A. Rauf, R. Jin and E. Hussain, *Nanoscale*, 2024, **16**, 7154–7166.
16 F. Saleem, M. Z. Abid, K. Rafiq, A. Rauf, K. Ahmad, S. Iqbal, R. Jin and E. Hussain, *Int. J. Hydrogen Energy*, 2024, **52**, 305–319.
17 J. Ran, J. Zhang, J. Yu, M. Jaroniec and S. Z. Qiao, *Chem. Soc. Rev.*, 2014, **43**, 7787–7812.
18 K. U. Sahar, K. Rafiq, M. Z. Abid, U. ur Rehman, A. Rauf and E. Hussain, *React. Chem. Eng.*, 2023, **8**, 2522–2536.
19 M. Sabir, K. Rafiq, M. Z. Abid, U. Quyyum, S. S. A. Shah, M. Faizan, A. Rauf, S. Iqbal and E. Hussain, *Fuel*, 2023, **353**, 129196.
20 M. Z. Abid, A. Ilyas, K. Rafiq, A. Rauf, M. A. Nadeem, A. Waseem and E. Hussain, *Environ. Sci.: Water Res. Technol.*, 2023, **9**, 2238–2252.
21 E. Hussain, I. Majeed, M. A. Nadeem, A. Badshah, Y. Chen, M. A. Nadeem and R. Jin, *J. Phys. Chem. C*, 2016, **120**, 17205–17213.
22 E. Hussain, M. Jalil, M. Z. Abid, J. Mansab, R. H. Althomali, S. Wang, A. Rauf and K. Rafiq, *Mater. Adv.*, 2024, **5**, 6572–6585.
23 P. Yadav, P. K. Dwivedi, S. Tonda, R. Boukherroub and M. V. Shelke, *Green Photocatalysts*, 2020, pp. 89–132.
24 H. H. Do, T. H. C. Nguyen, T. Van Nguyen, C. Xia, D. L. T. Nguyen, P. Raizada, P. Singh, V.-H. Nguyen, S. H. Ahn and S. Y. Kim, *Int. J. Hydrogen Energy*, 2022, **47**, 37552–37568.
25 C. Zhang, H. Gao, G. Hai, Y. Zeng, X. Wang, L. Xing, J. Zhao, G. Wang and X. Shu, *J. Colloid Interface Sci.*, 2022, **607**, 1836–1848.

26 M. Z. Abid, K. Rafiq, A. Rauf, R. H. Althomali and E. Hussain, *Mater. Adv.*, 2024, **5**, 2238–2252.
27 Z. Abid, K. Rafiq, A. Rauf and E. Hussain, *Nanoscale Adv.*, 2024, **6**, 5861–5873.
28 Y. Nam, J. H. Lim, K. C. Ko and J. Y. Lee, *J. Mater. Chem. A*, 2019, **7**, 13833–13859.
29 A. B. Djurišić, Y. He and A. Ng, *APL Mater.*, 2020, **8**, 030903.
30 L. Cheng, Q. Xiang, Y. Liao and H. Zhang, *Energy Environ. Sci.*, 2018, **11**, 1362–1391.
31 B. Kundu, A. S. Shajahan, B. Chakraborty, R. K. Behera, M. K. Sarangi, D. Pradhan and P. K. Sahoo, *ACS Appl. Nano Mater.*, 2023, **6**, 23078–23089.
32 H. Duan and Y. Xuan, *Phys. E*, 2011, **43**, 1475–1480.
33 S. Chen, D. Huang, P. Xu, W. Xue, L. Lei, M. Cheng, R. Wang, X. Liu and R. Deng, *J. Mater. Chem. A*, 2020, **8**, 2286–2322.
34 P. Kumari, N. Bahadur, L. Kong, L. A. O'Dell, A. Merenda and L. F. Dumée, *Mater. Adv.*, 2022, **3**, 2309–2323.
35 H. Choi, S.-J. Ko, Y. Choi, P. Joo, T. Kim, B. R. Lee, J.-W. Jung, H. J. Choi, M. Cha and J.-R. Jeong, *Nat. Photonics*, 2013, **7**, 732–738.
36 S. G. Kumar, R. Kavitha and P. Nithya, *J. Environ. Chem. Eng.*, 2020, **8**, 104313.
37 N. L. Reddy, V. N. Rao, M. Vijayakumar, R. Santhosh, S. Anandan, M. Karthik, M. Shankar, K. R. Reddy, N. P. Shetti and M. Nadagouda, *Int. J. Hydrogen Energy*, 2019, **44**, 10453–10472.
38 C. de Melo, M. Jullien, Y. Battie, A. En Naciri, J. Ghanbaja, F. Montaigne, J.-F. Pierson, F. Rigoni, N. Almqvist and A. Vomiero, *ACS Appl. Mater. Interfaces*, 2018, **10**, 40958–40965.
39 N. Güy, *Appl. Surf. Sci.*, 2020, **522**, 146442.
40 Y. Liu, Z. Sun and Y. H. Hu, *Chem. Eng. J.*, 2021, **409**, 128250.
41 W. Wang, H. Lin, J. Li and N. Wang, *J. Am. Ceram. Soc.*, 2008, **91**, 628–631.
42 M. Rezaei, A. Nezamzadeh-Ejhieh and A. R. Massah, *Energy Fuels*, 2024, **38**, 7637–7664.
43 S. Ismail, M. Sahar and S. Ghoshal, *Mater. Res. Bull.*, 2016, **74**, 502–506.
44 B. G. T. Keerthana and P. Murugakoothan, *Vacuum*, 2019, **159**, 476–481.
45 S. Patnaik, G. Swain and K. Parida, *Nanoscale*, 2018, **10**, 5950–5964.
46 X. Meng, C. Zhang, C. Dong, W. Sun, D. Ji and Y. Ding, *Chem. Eng. J.*, 2020, **389**, 124432.
47 F. Lin, Z. Wang, Q. Ma, Y. Yang, R. Whiddon, Y. Zhu and K. Cen, *Appl. Catal., B*, 2016, **198**, 100–111.
48 N. Zhang, S. Liu, X. Fu and Y.-J. Xu, *J. Mater. Chem.*, 2012, **22**, 5042–5052.
49 M. Cao, Y. Zou, Y. Zhang, T. Zeng, Q. Wan, G. Lai and N. Yang, *Electrochim. Acta*, 2022, **409**, 139967.
50 A. Pandey, S. Dalal, S. Dutta and A. Dixit, *J. Mater. Sci.: Mater. Electron.*, 2021, **32**, 1341–1368.
51 E. I. Altman, M. Z. Baykara and U. D. Schwarz, *Acc. Chem. Res.*, 2015, **48**, 2640–2648.
52 J. M. Cerrato, M. F. Hochella Jr, W. R. Knocke, A. M. Dietrich and T. F. Cromer, *Environ. Sci. Technol.*, 2010, **44**, 5881–5886.
53 E. Hussain, A. Ishaq, M. Z. Abid, M. Z. Waleed, A. Rauf, R. Jin and K. Rafiq, *ACS Appl. Energy Mater.*, 2024, **7**, 1914–1926.
54 M. Wang, P. Ma, Z. Wu, S. Chu, Y. Zheng, Z. Zhou and W. Weng, *Appl. Surf. Sci.*, 2022, **599**, 153897.
55 T. Senasu, K. Hemavibool and S. Nanan, *RSC Adv.*, 2018, **8**, 22592–22605.
56 A. Malankowska, A. Mikołajczyk, J. Mędrzycka, I. Wysocka, G. Nowaczyk, M. Jarek, T. Puzyn and E. Mulkiewicz, *Environ. Sci.:Nano*, 2020, **7**, 3557–3574.
57 X. Lu, W. Chen, Y. Yao, X. Wen, J. N. Hart, C. Tsounis, C. Y. Toe, J. Scott and Y. H. Ng, *Chem. Eng. J.*, 2021, **420**, 127709.
58 C. Xue, X. Yan, H. An, H. Li, J. Wei and G. Yang, *Appl. Catal., B*, 2018, **222**, 157–166.
59 J. A. Nasir, Z. ur Rehman, S. N. A. Shah, A. Khan, I. S. Butler and C. R. A. Catlow, *J. Mater. Chem. A*, 2020, **8**, 20752–20780.
60 Y. Lu, R. Jin, Y. Qiao, W. Liu, K. Wang, X. Wang and C. Wang, *Int. J. Electrochem. Sci.*, 2020, **15**, 10243–10252.
61 X. Ning and G. Lu, *Nanoscale*, 2020, **12**, 1213–1223.
62 Y. H. Sim, M. J. Yun, L. Fauzan, H. Choi, D. Y. Lee and S. I. Cha, *Sustainable Energy Fuels*, 2024, **8**, 700–716.
63 D. Xu, S.-N. Zhang, J.-S. Chen and X.-H. Li, *Chem. Rev.*, 2022, **123**, 1–30.
64 M. Sabir, K. Rafiq, M. Z. Abid, U. Quyyum, S. S. A. Shah, M. Faizan, A. Rauf, S. Iqbal and E. Hussain, *Fuel*, 2023, **353**, 129196.
65 K. Rafiq, M. Sabir, M. Z. Abid, M. Jalil, M. A. Nadeem, S. Iqbal, A. Rauf and E. Hussain, *Energy Fuels*, 2024, **38**, 4625–4636.
66 C. Zhu, C. A. Liu, Y. Fu, J. Gao, H. Huang, Y. Liu and Z. Kang, *Appl. Catal., B*, 2019, **242**, 178–185.
67 W. Li, J. Han, Y. Wu, Q. Xiang, Y. Qiao, C. Feng, Z. Chen and X. Deng, *Mater. Lett.*, 2019, **255**, 126560.
68 F. Wang, C. Hu, C. Chen, S. Cao, Q. Li, Y. Wang and J. Ma, *Appl. Surf. Sci.*, 2023, **614**, 156190.
69 J. Zhong, Y. Li, H. Zhang, Z. Zhang, K. Qi, H. Zhang, C. Gao, Y. Li, L. Wang, Z. Sun, C. Zhuang and X. Han, *J. Colloid Interface Sci.*, 2023, **630**, 260–268.
70 W. Tan, Y. Li, W. Jiang, C. Gao and C. Zhuang, *ACS Appl. Energy Mater.*, 2020, **3**, 8048–8054.
71 Y. Leng, J. Liu, C. Zhang and P. Jiang, *Catal. Sci. Technol.*, 2014, **4**, 997–1004.
72 Y. Wang, H. Suzuki, J. Xie, O. Tomita, D. J. Martin, M. Higashi, D. Kong, R. Abe and J. Tang, *Chem. Rev.*, 2018, **118**, 5201–5241.
73 C. Jiang, S. J. Moniz, A. Wang, T. Zhang and J. Tang, *Chem. Soc. Rev.*, 2017, **46**, 4645–4660.
74 W. Fan, B. Zhang, X. Wang, W. Ma, D. Li, Z. Wang, M. Dupuis, J. Shi, S. Liao and C. Li, *Energy Environ. Sci.*, 2020, **13**, 238–245.
75 Y. Wang, W. Zhang, D. Li, J. Guo, Y. Yu, K. Ding, W. Duan, X. Li, H. Liu and P. Su, *Adv. Sci.*, 2021, **8**, 2004456.

76 S. Pansri, R. Supruangnet, H. Nakajima, S. Rattanasuporn and S. Noothongkaew, *J. Mater. Sci.*, 2020, **55**, 4332–4344.
77 A. J. Esswein and D. G. Nocera, *Chem. Rev.*, 2007, **107**, 4022–4047.
78 Y. Quan, G. Wang, C. Chang and Z. Jin, *Nanoscale*, 2023, **15**, 1186–1199.
79 J. L. Wang and L. J. Xu, *Crit. Rev. Environ. Sci. Technol.*, 2012, **42**, 251–325.
80 W. Yu, Z. Chen, Y. Fu, W. Xiao, B. Dong, Y. Chai, Z. Wu and L. Wang, *Adv. Funct. Mater.*, 2023, **33**, 2210855.
81 U. Quyyum, K. Rafiq, M. Z. Abid, F. Ahmad, A. Rauf and E. Hussain, *Environ. Sci.: Water Res. Technol.*, 2023, **9**, 1147–1160.
82 J. Yu, Z. Chen, L. Zeng, Y. Ma, Z. Feng, Y. Wu, H. Lin, L. Zhao and Y. He, *Sol. Energy Mater. Sol. Cells*, 2018, **179**, 45–56.
83 H.-Y. Xu, S.-Q. Zhang, Y.-F. Wang, Y. Xu, L.-M. Dong and S. Komarneni, *Appl. Surf. Sci.*, 2023, **614**, 156225.
84 P. Setiani, N. Watanabe, R. R. Sondari and N. Tsuchiya, *Mater. Renewable Sustainable Energy*, 2018, **7**, 1–13.
85 S.-i. Fujita, H. Kawamori, D. Honda, H. Yoshida and M. Arai, *Appl. Catal., B*, 2016, **181**, 818–824.
86 S. Kampouri and K. C. Stylianou, *ACS Catal.*, 2019, **9**, 4247–4270.
87 N. Gupta and B. Pal, *J. Mol. Catal. A: Chem.*, 2014, **391**, 158–167.
88 M. Z. Rahman, K. Davey and C. B. Mullins, *Adv. Sci.*, 2018, **5**, 1800820.
89 K. Rafiq, K. U. Sahar, M. Z. Abid, S. Attique, U. U. Rehman, A. Rauf and E. Hussain, *Energy Adv.*, 2024, **3**(5), 983–996.